

Estimations of Evapotranspiration and Water Balance with Uncertainty over the Yukon River Basin

Wenping Yuan · Shuguang Liu · Shunlin Liang · Zhengxi Tan · Heping Liu · Claudia Young

Received: 27 November 2010 / Accepted: 22 February 2012 /
Published online: 14 March 2012
© Springer Science+Business Media B.V. 2012

Abstract In this study, the revised Remote Sensing-Penman Monteith model (RS-PM) was used to scale up evapotranspiration (ET) over the entire Yukon River Basin (YRB) from three eddy covariance (EC) towers covering major vegetation types. We determined model parameters and uncertainty using a Bayesian-based method in the three EC sites. The 95 % confidence interval for the aggregate ecosystem ET ranged from 233 to 396 mm yr⁻¹ with an average of 319 mm yr⁻¹. The mean difference between precipitation and evapotranspiration

W. Yuan · S. Liang

State Key Laboratory of Remote Sensing Science, Jointly Sponsored by Beijing Normal University and Institute of Remote Sensing Applications, Chinese Academic of Science, Beijing 100875, China

W. Yuan (✉) · S. Liang

College of Global Change and Earth System Science, Beijing Normal University, Beijing 100875, China
e-mail: wenpingyuancn@yahoo.com

S. Liu

United States Geological Survey (USGS) Earth Resources Observation and Science (EROS) Center, Sioux Falls, SD 57198, USA

S. Liu

Geographic Information Science Center of Excellence, South Dakota State University, Brookings, SD 57007, USA

Z. Tan

ASRC Research and Technology Solutions, Contractor to the USGS Earth Resources Observation and Science (EROS) Center, Sioux Falls, SD, USA

H. Liu

Department of Civil & Environmental Engineering, Washington State University, Pullman, WA 99164, USA

C. Young

ADNET Systems, Inc., Contractor to the USGS Earth Resources Observation and Science (EROS) Center, Sioux Falls, SD, USA

S. Liang

Department of Geography, University of Maryland, College Park, MD 20742, USA

(W) was 171 mm yr^{-1} with a 95 % confidence interval of $94\text{--}257 \text{ mm yr}^{-1}$. The YRB region showed a slight increasing trend in annual precipitation for the 1982–2009 time period, while ET showed a significant increasing trend of $6.6 \text{ mm decade}^{-1}$. As a whole, annual W showed a drying trend over YRB region.

Keywords Evapotranspiration · Bayesian approach · Markov chain Monte Carlo · Model uncertainty · Yukon river basin

1 Introduction

A high-latitude region is of particular interest and important to the global water cycle because of climate change (Zhang et al. 2009). Numerous of studies have shown that high-latitude regions experience increased precipitation and temperature (IPCC 2007). As a consequence, increasing evidences indicate substantial changes at the regional water balance (Franchini et al. 2011; Zhang et al. 2009), which strongly effect ecological processes in this domain.

Ecosystem evapotranspiration (ET) is a fundamental process linking hydrologic, atmospheric, and ecological processes. On average, nearly two thirds of precipitation that falls over global land is returned to the atmosphere via ET. However, ET is the most problematic component of the water cycle to be accurately estimated because of the heterogeneity of the landscape and the large number of controlling factors involved, including climate, plant biophysics, soil properties, and topography (Dirmeyer et al. 2006). Many studies have analyzed the effects of propagating parameter uncertainty in ecosystem water cycle models; however, most of these studies have used a local design, i.e., changing one parameter at a time within a given range around the standard value (Knorr and Heimann 2001), or using minimum and maximum values from the literature (Hassaballah et al. 2012). Although these approaches can identify the main effects of parameters, they neglect possible interactions between different parameters, which are important in complex ecosystem models. In addition, few studies determined simulation uncertainties across regional scales because such assessments require many model executions, which are prohibitive for complex models with a large number of parameters and high computational demand (Campolongo et al. 2000).

We adopt a Bayesian-based method, which used the Monte Carlo-type stratified sampling approach Metropolis-Hastings (MH) as an efficient method to identify functionally important parameters and to simultaneously estimate the uncertainty range of the modeled results. Like other probability-based methods, MH allows interactions between different parameter combinations to be studied and can identify the contributions of parameters alone and in combination with the uncertainty of the modeled results. MH has been shown to provide reliable estimates of the distribution function of model output variables (Helton and Davis 2000). In addition, a simple method was developed to determine parameter uncertainty for regional simulations (see the method).

The study area for this research encompasses the Yukon River Basin (YRB) (Fig. 1a), which covers approximately $840,000 \text{ km}^2$ and is predominantly composed of boreal forest and northern temperate grassland. The Yukon River is one of the largest rivers in the northern regions. It contributes $203 \text{ km}^3 \text{ yr}^{-1}$ freshwater to the Bering Sea. The primary objectives of this paper were (1) to derive ecosystem ET model parameters at three ecosystems of the YRB and determine parameter uncertainties; (2) to estimate ET and predict uncertainty over the YRB considering parameter uncertainty; and (3) to assess spatial patterns and temporal trends in ET and water balance over the YRB from 1982 to 2009.

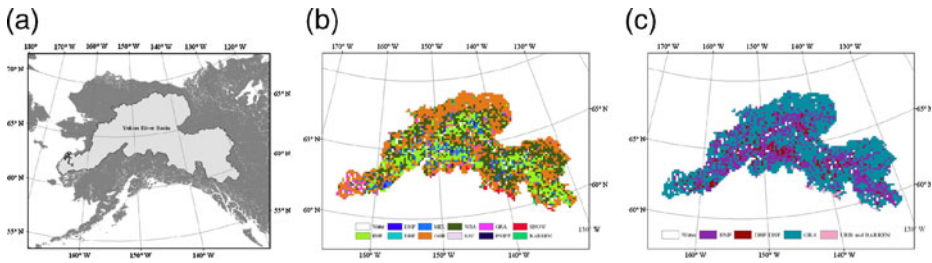


Fig. 1 Map of study region and land cover derived from the IGBP-MODIS global land cover classification for Yukon River Basin. **a** Location map of Yukon River Basin; **b** the original land cover map and **c** aggregated land cover map for the Yukon River Basin. The original eight land cover types aggregate to three types: Evergreen Needleleaf Forest (ENF) only including Evergreen Needleleaf Forest; Deciduous Broadleaf Forest (DBF) including Deciduous Needleleaf Forest (DNF), DBF and Mixed Forest (MF); Grassland (GRS) including Open Shrubland (OSH), Woody Savannas (WSV), Savannas (SAV), Grasslands (GRS), Permanent Wetlands (PWET). SNOW indicates snow and ice, and Barren indicates barren or sparsely vegetated cover types. Areas in white represent open water and other areas outside the study area

2 Method and Data

2.1 Revised Remote Sensing-Penman Monteith (RS-PM) Model

The ecosystem ET model used in this study was the revised Remote Sensing-Penman Monteith (RS-PM) model. The RS-PM model was originally proposed by Cleugh et al. (2007) and revised by Mu et al. (2007). Yuan et al. (2010) revised the equations dealing with temperature constraint for stomatal conductance and energy allocation between vegetation canopy and soil surface. In total, three parameters, VPD_{close} (vapor pressure deficit threshold value for full stomatal closure, k Pa), C_{tot} (total aerodynamic conductance to vapor transport, $m s^{-1}$) and C_L (mean potential stomatal conductance, $m s^{-1}$), governed the model's behavior, and were calibrated using observed ET from eddy flux towers (please see Yuan et al. (2010)).

2.2 Eddy Flux Measurements for Model Calibration

Three adjacent eddy covariance (EC) towers in the interior YRB, were used in this study: Burn1999 (63°55'N, 145°44'W), Burn1987 (63°55'N, 145°23'W) and Control (63°53'N, 145°44'W). These three EC towers measured the fluxes of sensible heat (H) and latent heat (LE) in deciduous broadleaf forest (Burn1987), evergreen needleleaf forest (Burn1999), and grassland (Control) from January 2002 to September 2004 (Liu and Randerson 2008). We filled short data gaps of LE (<3 h) with linear interpolation and we used the mean diurnal method for filling longer gaps (Falge et al. 2001). Liu and Randerson (2008) showed the energy closure at these three sites within the range of those reported by the FLUXNET community (Wilson et al. 2002).

2.3 Meteorology and Remote Sensing Data over the YRB

We chose 1982–2009 as the study period for estimating regional ET based on the satellite-observed vegetation attributes and daily surface meteorology inputs. To produce a

continuous and consistent time series LAI from 1982 to 2009, we combined Advanced Very High Resolution Radiometer (AVHRR) LAI and MODIS LAI which were acquired from different sensors. The AVHRR LAI products, with 16-km resolution from 1982 to 2000, are based on a monthly maximum value compositing of AVHRR spectral reflectance data to mitigate cloud cover, smoke, and other atmospheric aerosol contamination effects (<http://cybele.bu.edu>; Myneni et al. 1997). The 8-day MODIS LAI (MOD15A2) data were used in this study from 2000 to 2009. QC flags were examined to screen and reject LAI data with insufficient quality. We temporally filled the missing or unreliable LAI at each 1-km MODIS pixel based on their corresponding quality assessment data fields as proposed by Zhao et al. (2005). MODIS LAI data were aggregated to 16-km spatial resolution, and the monthly maximum values were indicated as LAI values of a given month. Linear regression method was used to combine the two LAI series into a single and continuous record (Zhang et al. 2008). Zhang et al. (2008) validated the combined AVHRR-MODIS LAI time series, and both error distribution and correlation analyses indicate that the approach for combining AVHRR and MODIS LAI time series is reliable.

We used input data sets of net radiation (R_n), air temperature (T), relative humidity (R_h), and photosynthetically active radiation (PAR) from the Modern Era Retrospective-Analysis for Research and Applications (MERRA) archive for 1982–2009 at a resolution of 0.5° latitude by 0.6° longitude. Because of the availability of AVHRR LAI at 16-km resolution, we adopted this resolution for the ET calculation and associated analysis.

The International Geosphere–Biosphere Programme (IGBP) 17-class MODIS Type 1 global land cover map (Friedl et al. 2002) is available at 1-km resolution and was aggregated to 16-km resolution to define general biome biophysical properties within the YRB (Fig. 1b). We aggregated the original eight IGBP land cover types to three major regional ecosystem types: evergreen needleleaf forest, deciduous broadleaf forest, and grassland (Fig. 1c).

2.4 Model Parameters Inversion with Markov Chain Monte Carlo (MCMC) Approach

To execute the data-model assimilation, we first specified ranges for model parameters as prior knowledge. The initial values and the lower and upper boundaries of the parameters were defined according to values reported in Kelliher et al. (1995). The initial, lower and upper values are 0.01 ms^{-1} , 0.002 ms^{-1} , 0.1 ms^{-1} for C_{tot} , 0.005 ms^{-1} , 0.0002 ms^{-1} , 0.01 ms^{-1} for C_l , and 2kPa, 0kPa, 5 kPa for VPD_{close} respectively. We then used MCMC technique to generate high-dimensional PDFs of model parameters via a sampling procedure. After we run the model 100,000 times, the model parameters estimated by the MH algorithm converged to stationary distributions.

To quantify prediction uncertainty at regional scale from parameter uncertainties, it is impossible to use all accepted model parameters from 100,000-time executions from site to region because of the high computational demand to run that many executions at all pixels. A simple method was used to determine the optimal model parameters and their uncertainties for other grids at the YRB. Cumulative probability curves for each parameter were generated based on probability distribution, and then were normalized to the range from 0 to 1. One thousand random numbers were generated ranging from 0 to 1 for indicating normalized cumulative probability value, and the corresponding parameter values were used to simulate ET. From the statistical standpoint, the probability of selecting optimal values for each parameter is high, which assures the same probability distribution of selected parameters with all accepted model parameters from 100,000-time executions at the MCMC.

2.5 Trend Analysis

Linear trend analysis was used to analyze regional trends in the hydrological variables (y_t). The linear model, $y_t = bt + y_0$, is used to model y_t against time (t), and b and y_0 are the slope and intercept of the regression line, respectively. The statistic $b/SE(b)$ has a Student's t -distribution, and the Student's t -test was used to analyze and classify trend significance into weak, moderate, and strong categories. When $|b/SE(b)| < 1.0$, i.e., b is within one standard deviation, the trend is classified as weak; when $1.0 \leq |b/SE(b)| \leq t_{0.10}$ where $t_{0.10}$ is the 10 % critical value of the Student's t -distribution, the trend is classified as moderate; when $|b/SE(b)| \geq t_{0.10}$, the trend is statistically significant and classified as strong. These categories were further stratified into six classes according to the slopes of the statistical trends: positive weak, positive moderate, positive strong, negative weak, negative moderate, and negative strong.

3 Results

3.1 Inversed Parameters and Model Performance at the Three EC Sites

The model successfully simulated ET at the three ecosystems with the R^2 between measured and modeled ET above 0.8 (Data not shown). C_{tot} , C_L , and VPD_{close} were estimated at the three EC sites using the MCMC method. At all three ecosystem types, three parameters were well constrained within their prespecified ranges (Fig. 2). Comparison of posterior mean of

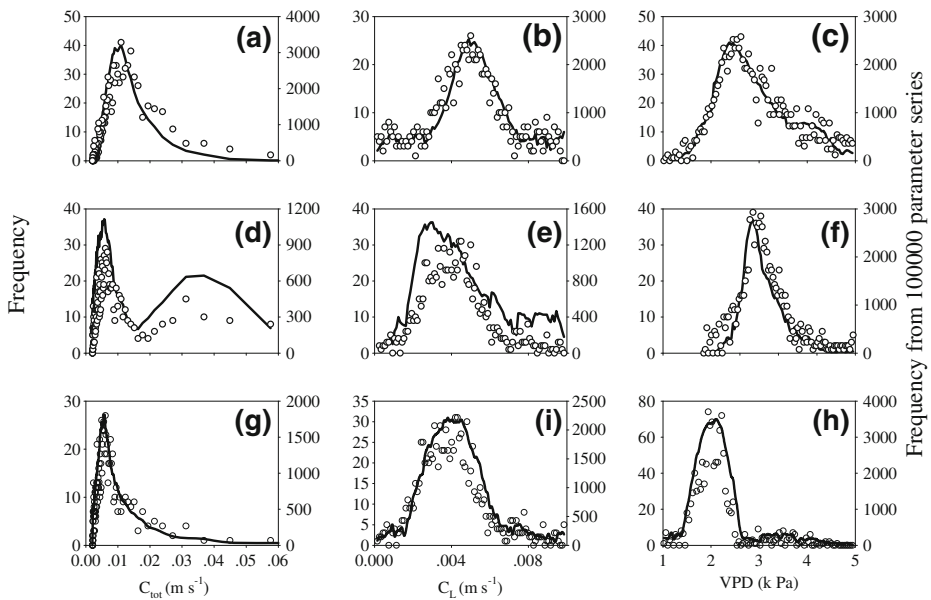


Fig. 2 Histogram to indicate frequency distribution of parameters derived from the Bayesian inversion with 100,000 parameter sampling series by the MH algorithm (solid lines) and 1000 randomly selected parameters based on normalized cumulative probability function curves (open dots). **a–c**, **d–f** and **g–h** show three parameters at the Burn87, Burn99, and Control sites. C_{tot} (total aerodynamic conductance to vapor transport, m s⁻¹) and C_L (mean potential stomatal conductance, m s⁻¹), and VPD_{close} (vapor pressure deficit threshold value for full stomatal closure, k Pa)

parameter shows that C_{tot} and C_L were much higher at Burn87 than Burn99 and Control sites (Fig. 2). No clear difference was found for parameter VPD_{close} . The randomly selected 1000 parameters show a similar probability distribution with that derived from all 100,000-time executions (Fig. 2).

3.2 Spatial Patterns of ET and Water Balance with Uncertainty

The model-based annual ET patterns are spatially complex and showed the largest ET in the central YRB (Fig. 3a). The spatial pattern of ET also corresponds to distributions of the major biome types. Deciduous broadleaf forests have the highest annual ET

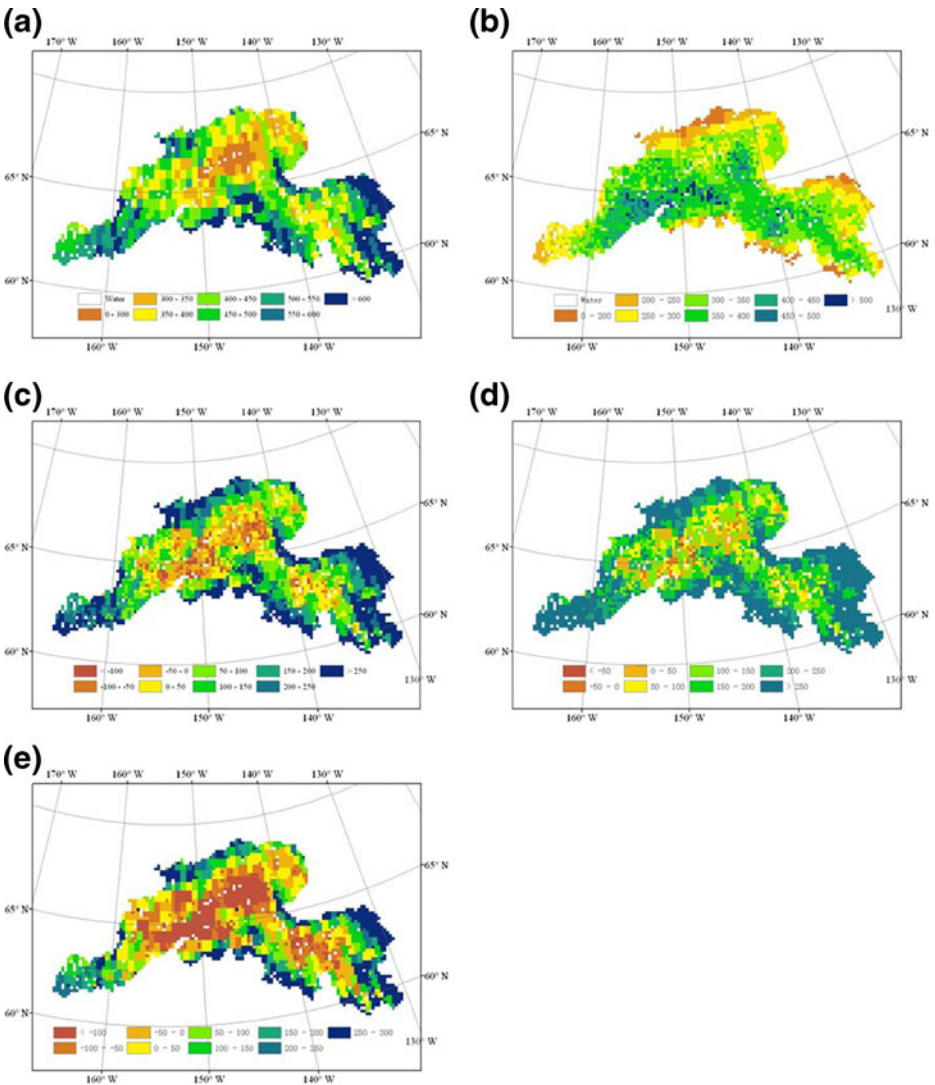


Fig. 3 Maps of multiyear (1982–2009) annual mean ET derived by optimal parameters **a**, annual mean P **b**, difference between P and ET derived from the optimal **c**, minimum **d**, and maximum estimated parameters **e**

($353 \pm 58 \text{ mm yr}^{-1}$) among the three major biome types followed by evergreen needleleaf forests ($326 \pm 47 \text{ mm yr}^{-1}$) and grasslands ($312 \pm 68 \text{ mm yr}^{-1}$). The confidence interval of 95 % for continentally aggregated ecosystem ET ranged from 233 to 396 mm yr^{-1} , with an average of 319 mm yr^{-1} .

The ET results were aggregated to annual fluxes and used precipitation (P) to evaluate recent changes in the regional water balance (W). On average, ET represents 65 ± 6 % of P in the YRB. Large differences were found in W derived by minimum and maximum simulated ET. 37.69 % and 1.50 % of areas where negative W occurred are indicated by the maximum and minimum ET range, respectively (Fig. 3c, d, e). The mean W for the YRB region is 171 mm yr^{-1} with a 95 % confidence interval of $94\text{--}257 \text{ mm yr}^{-1}$.

3.3 Temporal Patterns of ET and Water Balance

ET shows a significant positive trend of $6.6 \text{ mm decade}^{-1}$ ($P < 0.05$) over the whole YRB region (Data not shown). Approximately, 54 % of areas over YRB represent moderate to strong positive ET trends (Fig. 4a). As a whole, the YRB region shows a slight positive trend in annual P for the 1982–2009 period (Data not shown). There is considerable spatial variability in P for the domain (Fig. 4b). The results show respective positive P trends for 55 % of the domain, while moderate to strong positive precipitation trends occur over 20 % of the region. On the contrary, 45 % of areas showed negative trends, and areas with strong negative precipitation trends primarily occur in the center Alaska.

Both P and ET show positive trends so the net effect on the difference between P and ET is reduced and annual W shows an insignificant drying trend (Data not shown). Areas showing moderate to strong positive W trends account for 14 % of the whole YRB region (Fig. 4c). Some areas have experienced drying trends during this period, including portions of central YRB (Fig. 4c). Areas of moderate and strong negative W trends account for 25 % of YRB region. For spatial pattern, drying trends mostly occur at regions with decreasing precipitation.

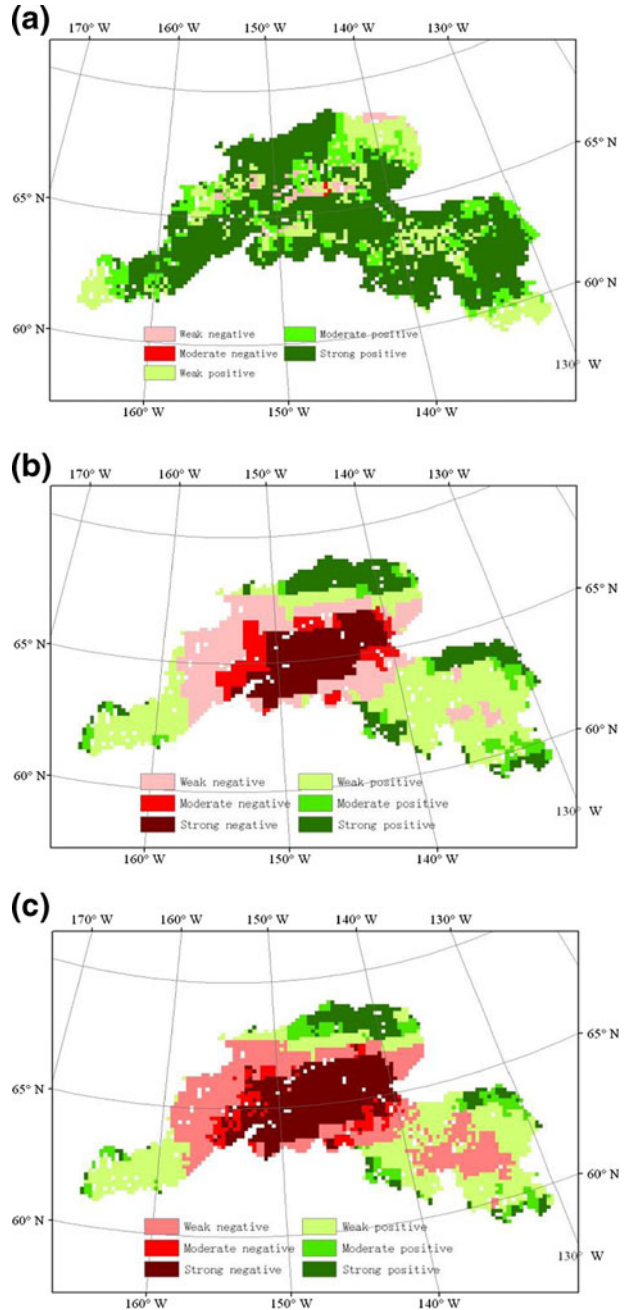
4 Discussions

4.1 Temporal and Spatial Patterns of ET and Water Balance over the YRB Region

ET varied greatly among the three ecosystems. On average, at the annual scales, ET was significantly higher in deciduous broadleaf forest ($353 \pm 58 \text{ mm yr}^{-1}$) than in evergreen needleleaf forest ($326 \pm 47 \text{ mm yr}^{-1}$) and grassland ($312 \pm 68 \text{ mm yr}^{-1}$), which were consistent with previous studies (Kljun et al. 2006). Other lines of evidence have supported this conclusion that ET is less at conifer stands than deciduous broadleaf forests (Baldocchi et al. 1997) because stomatal conductance has been observed to remain fairly constant over a wide range of vapour pressure deficit (VPD) in evergreen needleleaf forest (Ewers et al. 2005). On the other hand, deciduous broadleaf forests are more sensitive to conditions of high evaporative demand at the leaf level (Hogg et al. 2000). In this study, the inverted parameters (i.e. C_{tot} and C_i) also showed the highest aerodynamic and potential stomatal conductance to vapor transport (Fig. 2). Therefore, the simulations of ET based on site-specific parameters inverted from EC measurements will improve the regional simulations.

The difference between P and ET results show large spatial discrepancies over the YRB region (Fig. 3). On average, the results show a positive water surplus of $170 \pm 40 \text{ mm yr}^{-1}$.

Fig. 4 Spatial distributions of trends in annual ET (a), P (b), and P-ET (c) within the YRB from 1982 to 2009. The trends are classified into six categories according to statistical linear trend analysis



Approximately, 17 %, 55 %, and 12 % of areas with water deficit occur over evergreen needleleaf forest, deciduous broadleaf forest, and grassland, respectively. The frequency of fires is also projected to increase in the future (Flannigan et al. 2005), which will increase the relative abundance of early- to mid-successional deciduous stands (Chapin et al. 2000), leading to an increase of ET at the regional scale.

The annual pattern of ET predicted by the revised RS-PM model over the years 1982–2009 shows a significant increase in annual ET flux from about 315 mm yr⁻¹ to almost 327 mm yr⁻¹. The ET results show generally positive trends for the YRB region; approximately 54 % of areas with positive ET trends occur over the region. Zhang et al. (2009) showed similar results at most areas of the pan-Arctic domain, especially boreal regions of North America.

Over the whole YRB, there are not significant changing trends in P and the difference between P and ET (W). However, from the spatial scale, the P and W present the significant changing trends. The results show 45 % of areas with negative P trends over the study region, and 22 % of areas show a moderate to strong negative trend. Derived by P and ET changes, 25 % of areas show that moderate and strong negative W trends, primarily occur in central YRB. We found our general drying trends for the YRB region are generally consistent with recent reports of widespread drought over northern regions due to increases in evaporative water losses (Zhang et al. 2009).

The impacts of droughts on boreal vegetation are also documented in other studies (Godden et al. 2011). In Alaska, tree-ring studies show a reduction in the growth of white spruce (Barber et al. 2004), even at some upper tree-line sites (Wilhite et al. 2007), because of a recent increase in temperature-induced drought stress. Hogg and Wein (2005) also reported recent drought-induced reductions in forest growth and regeneration in southwestern Yukon, Canada. A previous study showed that the response of interior forest areas to temperature change has been inconsistent with expectations of direct positive relationships between plant growth and either warming or CO₂ concentration (Goetz et al. 2005). Emerging evidence shows that drought stress is a key factor for this apparent decoupling of growth and warming in northern regions (Barber et al. 2004; Wilhite et al. 2007). Therefore, it should be widely realized that drought has altered the ecosystem structure and function, and it must be accounted for ecosystem management (Klos et al. 2009).

4.2 Effects of Parameter Uncertainties on the Modeling of ET

Many studies have shown that the uncertainty of model parameters was the largest contributor to the overall model uncertainty compared with other various sources (e.g., inputs, observations, model structure) (Verbeeck et al. 2006). Therefore, the assessment of the uncertainty surrounding estimates of evaporation provides extremely useful information for water resource management and investigations on impacts of water in ecosystems. At the maximum and minimum range of simulated ET determined by the parameter uncertainty, there are larger differences between model water balances (W).

In this study, a sample size of 1000 sets was generated to indicate, for each model output variable, a reliable estimate of the mean, standard deviation, and 90 % confidence interval based on parameter cumulative probability functions. The parameters are likely to be interdependent to a greater or lesser extent, for example, because of the existence of structural and functional characteristics. In our analyses, we randomly selected parameters based on normalized cumulative probability functions individually without assuming any interdependence. This might cause overestimation of uncertainty, and thereby unjustifiably reduce confidence in model results (Helton and Davis 2000). To examine the overestimation, we compared the prediction uncertainty using 1000 sample sets with all 100,000 sets of parameters. The results showed there are not significant differences of ET estimations using two sets of parameters (data not shown), which implied our methods effectively avoided the overestimations of parameter uncertainty and model bias without considering interdependence of parameters.

This study was focused on the uncertainty in process-based ecosystem evapotranspiration models due to imperfect knowledge of the “correct” parameter values used in scaled representations of ecosystem processes, and it aims to provide quantitative information about the confidence that can be placed in model results. However, other aspects of model uncertainty were not addressed; for example, uncertainty due to incomplete knowledge of the true mechanisms underlying certain ecosystem phenomena, as well as uncertainty in the driving environmental data, which may be equally important (Knorr and Heimann 2001). Future steps toward a quantitative assessment of the uncertainty in modeling terrestrial biosphere dynamics will need to account for uncertainty related to model assumptions and to consider driving factors.

5 Summary

We presented an assessment of parameter-based uncertainty in modeling ecosystem ET over the YRB from 1982 to 2009 using the revised RS-PM model. We then analyzed associated changes in the regional water balance defined as precipitation minus ET. ET showed generally positive trends over most of the YRB, but negative ET trends occurred over 46 % of the region. Increasing water deficits (difference between precipitation and ET) in the YRB agrees with regional drought records and recent satellite observations of vegetation browning and productivity reduction. Moreover, our results indicate prediction uncertainty derived from parameter uncertainties have large impacts on estimating regional water balance. Based on our analysis, we recommend that uncertainty analyses should be an integral part of the development and validation process for all process-oriented ecosystem models.

Acknowledgments This research was financially supported by the National Key Basic Research and Development Plan of China (2010CB833504), National High Technology Research and Development Program of China (863 Program) (2009AA122100) and Fundamental Research Funds for the Central Universities.

References

- Baldocchi DD, Vogel CA, Hall B (1997) Seasonal variation of energy and water vapor exchange rates above and below a boreal jack pine forest. *J Geophys Res* 102:28939–28952
- Barber VA, Juday GP, Finney BP, Wilmking M (2004) Reconstruction of summer temperatures in interior Alaska from tree-ring proxies: evidence for changing synoptic climate regimes. *Clim Chang* 63:91–120
- Campolongo F, Kleijnen J, Andres T (2000) Screening Methods. In: Saltelli A, Chan K, Scott EM (eds) Sensitivity analysis. Wiley, Chichester, UK
- Chapin FS III, Mcguire AD, Randerson J et al (2000) Arctic and boreal ecosystems of western North America as components of the climate system. *Global Change Biol* 6:211–223
- Cleugh HA, Leuning R, Mu Q, Running SW (2007) Regional evaporation estimates from flux tower and MODIS satellite data. *Remote Sens Environ* 106:285–304
- Dirmeyer PA, Gao X, Zhao M, Guo Z, Oki T, Hanasaki N (2006) GSWP-2: Multimodel analysis and implications for our perception of the land surface. *Bull Am Meteorol Soc* 87:1381–1397
- Ewers BE, Gower ST, Bond-Lamberty B, Wang CK (2005) Effects of stand age and tree species composition on transpiration and canopy conductance of boreal forest. *Plant Cell Environ* 28:660–678
- Falge E, Baldocchi D, Olson R et al (2001) Gap filling strategies for defensible annual sums of net ecosystem exchange. *Agr Forest Meteorol* 107:43–69
- Flannigan MD, Logan KA, Amiro BD, Skinner W, Stocks B (2005) Future area burned in Canada. *Clim Chang* 72:1–16

- Franchini M, Ventaglio E, Bonoli A (2011) A procedure for evaluating the compatibility of surface water resources with environmental and human requirements. *Water Resour Manage* 25:3613–3634
- Friedl MA, McIver DK, Hodges JCF et al (2002) Global land cover mapping from MODIS: algorithms and early results. *Remote Sens Environ* 83:287–302
- Godden L, Ison RL, Wallis PJ (2011) Water governance in a climate change world: appraising systemic and adaptive effectiveness. *Water Resour Manage* 25:3971–3976
- Goetz SJ, Bunn AG, Fiske GJ, Houghton RA (2005) Satellite-observed photosynthetic trends across boreal North America associated with climate and fire disturbance. *PNAS* 102:13521–13525
- Hassaballah K, Jonoski A, Popescu I, Solomatine DP (2012) Model-based optimization of downstream impact during filling of a new reservoir: case study of Mandaya/Roseires Reservoirs on the Blue Nile River. *Water Resour Manage* 26:273–293
- Helton JC, Davis FJ (2000) Sampling-based methods for uncertainty and sensitivity analysis. Sandia National Laboratories, Albuquerque
- Hogg EH, Price DT, Black TA (2000) Postulated feedbacks of deciduous forest phenology on seasonal climate patterns in the western Canadian interior. *J Clim* 13:4229–4243
- Hogg EH, Wein RW (2005) Impacts of drought on forest growth and regeneration following fire in southwestern Yukon, Canada. *Can J For Res* 35:2141–2150
- IPCC (2007) Climate Change 2007: The physical science basis. In: Solomon S, Qin D, Manning M, Chen Z, Marquis M, Averyt KB, Tignor M, Miller HL (eds) Contribution of Working Group I to the Fourth Assessment Report of the Intergovernmental Panel on Climate Change. Cambridge University Press, Cambridge
- Kelliher FM, Leuning R, Raupach MR, Schulze ED (1995) Maximum conductances for evaporation from global vegetation types. *Agr Forest Meteorol* 73:1–16
- Kljun NT, Black A, Griffis TJ et al (2006) Response of net ecosystem productivity of three boreal forest stands to drought. *Ecosystems* 10:1039–1055
- Klos RJ, Wang GG, Bauerle WL, Rieck JR (2009) Drought impact on forest growth and mortality in the southeast USA: an analysis using forest health and monitoring data. *Ecol Appl* 19:699–708
- Knorr W, Heimann M (2001) Uncertainties in global terrestrial biosphere modeling I: a comprehensive sensitivity analysis with a new photosynthesis and energy balance scheme. *Global Biogeochem Cy* 15:207–225
- Liu HP, Randerson JT (2008) Interannual variability of surface energy exchange depends on stand age in a boreal forest fire chronosequence. *J Geophys Res* 13:G01006. doi:10.1029/2007JG000483
- Mu QZ, Heinsch FA, Zhao MS, Running SW (2007) Development of a global evapotranspiration algorithm based on MODIS and global meteorology data. *Remote Sens Environ* 111:519–536
- Myneni RB, Keeling CD, Tucker CJ et al (1997) Increased plant growth in the northern high latitudes from 1981–1991. *Nature* 386:698–702
- Verbeeck H, Samson R, Verdonck F et al (2006) Parameter sensitivity and uncertainty of the forest carbon flux model FORUG: a monte carlo analysis. *Tree Physiol* 26:807–817
- Wilhite DA, Svoboda MD, Hayes MJ (2007) Understanding the complex impacts of drought: a key to enhancing drought mitigation and preparedness. *Water Resour Manage* 21:763–774
- Wilson K, Goldstein A, Falge E et al (2002) Energy balance closure at FLUXNET sites. *Agr Forest Meteorol* 113:223–243
- Yuan WP, Liu SG, Yu GR et al (2010) Global estimates of evapotranspiration and gross primary production based on MODIS and global meteorology data. *Remote Sens Environ* 114:1416–1431
- Zhang K, Kimball JS, Mu QZ et al (2009) Satellite based analysis of northern ET trends and associated changes in the regional water balance from 1983 to 2005. *J Hydrol* 379:92–110
- Zhang K, Kimball JS, Hogg EH et al (2008) Satellite-based model detection of recent climate-driven changes in northern high-latitude vegetation productivity. *J Geophys Res* 113:G03033. doi:10.1029/2007JG000621
- Zhao M, Heinsch FA, Nemani R, Running SW (2005) Improvements of the MODIS terrestrial gross and net primary production global data set. *Remote Sens Environ* 95:164–176